https://doi.org/10.5194/egusphere-2026-132
Preprint. Discussion started: 23 March 2026

Regularisation of the 4DEnVar Data Assimilation method for Calibration of Land Surface Models

Natalie Douglas[1*], Simon Beylat[2,3*], Tristan Quaife[1], Philippe Peylin[2], Nina Raoult[4], and Ross Bannister[1]

[1]National Centre for Earth Observation, Department of Meteorology, University of Reading, Reading, UK
[2]Laboratoire des Sciences du Climat et de l'Environnement, LSCE/IPSL, CEA-CNRS-UVSQ, Université Paris-Saclay, 91191 Gif-sur-Yvette, France
[3]School of Geography, Earth and Atmospheric Sciences, University of Melbourne, Parkville, 3010 Victoria, Australia
[4]European Centre for Medium-Range Weather Forecasts, Shinfield Park, Reading, UK
[*]These authors contributed equally to this work.

Correspondence: Natalie Douglas (n.douglas@reading.ac.uk) and Simon Beylat (simon.beylat@lsce.ipsl.fr)

Abstract. The four-dimensional ensemble variational (4DEnVar) data assimilation method is an attractive choice for land surface model calibration due to its ease of use, speed, and its circumvention of tangent linear model and adjoint calculations. However, in certain circumstances, this method may prove ineffective when implemented with a highly non-linear model, leading to out-of-range or non-physical posterior parameter values. To address this, the 4DEnVar cost function can be adapted through the introduction of a hyperparameter, which inflates the weight of the background term. In this study, we explore the anticipated challenges of applying 4DEnVar with in situ eddy-covariance flux measurements and present some explanations of the expected behaviour. We show that, when using a hyperparameter to regularise the optimisation, 4DEnVar is able to successfully calibrate two complex land surface models, JULES and ORCHIDEE, with comparable accuracy in its ability to produce model runs with an improved match to the observations. To our knowledge, this is the first study of its kind to compare parameter calibration of two different land surface models in the same experimental setting. In addition to the aforementioned benefits of using 4DEnVar, we show that the method also exhibits considerable versatility, not only with regard to the land surface model to which it is applied, but also in terms of parameter set selection and ensemble size.

1 Introduction

Climate models predict future Earth system changes and their potential impacts on human life based on increasing atmospheric CO_2 levels. These models integrate multiple components—including the atmosphere, oceans, and land surface—that interact to simulate the coupled climate system. Land surface models (LSMs), such as JULES (the Joint UK Land Environment Simulator; Best et al. (2011); Clark et al. (2011)) and ORCHIDEE (ORganizing Carbon and Hydrology In Dynamic EcosystEms; initially described by Krinner et al. (2005)), represent the land component by simulating exchanges of water, heat, and CO_2 with the atmosphere. These exchanges directly influence atmospheric processes and, consequently, climate projections. While LSMs are based on well-established physical principles for certain processes (e.g. interception of radiation), many biological processes (e.g. phenology) lack equations derived from first principles and must therefore rely on simplified or empirical representations

https://doi.org/10.5194/egusphere-2026-132
Preprint. Discussion started: 23 March 2026

(Fisher and Koven (2020), Blyth et al. (2021)). This results in many uncertain parameters that must be adjusted in order for LSM outputs to better compare with observations. Here, we give special attention to the photosynthetic processes of land surface models since carbon assimilation in terrestrial ecosystems constitutes a significant flux in the global carbon cycle.

Due to the advancement of computer technology and the advent of remotely sensed Earth system measurements, data assimilation (DA) techniques (Wang et al., 2001; Kaminski et al., 2002; Rayner et al., 2005; Santaren et al., 2007; Raoult et al., 2016) have been developed and evolved for parameter estimation in land surface modelling. Raoult et al. (2025) provide a comprehensive overview of the current challenges and potential opportunities for the DA techniques currently employed in land surface parameter estimation. In the case of complex LSMs, the classic 4DVar (4D-Variational) DA method (Rawlins et al., 2007) is an attractive method for model calibration, which has previously been implemented for JULES (Raoult et al., 2016) and ORCHIDEE (Kuppel et al., 2012; Bacour et al., 2015). However, this method requires complicated tangent linear and adjoint code calculation and maintenance, which is too demanding for models such as JULES and ORCHIDEE that are under constant development. While techniques that circumvent the need for tangent linear and adjoint models, such as finite differences, have been implemented (Santaren et al., 2007; Beylat et al., 2025), the 4DEnVar (4D Ensemble Variational) DA method (Liu et al., 2008) was designed to overcome these challenges by using an ensemble to approximate gradient information. The ensemble also provides an opportunity to easily obtain posterior parameter uncertainty information. In addition to these merits, the analysis step can be executed separately from model runs and is very quick to implement.

In this article, as well as in Pinnington et al. (2020, 2021); Douglas et al. (2025); Visweshwaran et al. (2025), we refer to this method exclusively as 4DEnVar. However, alternative names exist, such as the Ensemble Variational Data Assimilation method (EnVarDA), used in Beylat et al. (2025). Pinnington et al. (2020) introduced the name 'LAVENDAR' for the 4DEnVar method when applied to parameter calibration in land surface models and has been adopted by some of the JULES community (Pinnington et al., 2021; Visweshwaran et al., 2025). The term 4DEnVar originates from the work of Liu et al. (2008), who initially developed the method as En4DVar before renaming it to 4DEnVar in Liu and Xiao (2013). Nevertheless, the derivation of this method is very similar to methods used in other fields, which are known by different names, such as the Ensemble Kalman Filter (EnKF) (Peters et al., 2005), the Ensemble Transform Kalman Filter (ETKF) depending on the choice of square-root (Bishop et al., 2001) or the Iterative ensemble Kalman smoother (IEnKS) (Bocquet and Sakov, 2014). All these studies were conducted in the context of state estimation, but the ETKF was also used for parameter estimation in an idealised, low-dimensional cloud/convection model in Posselt and Bishop (2012), where it was compared with a Markov Chain Monte Carlo (MCMC) algorithm. This study showed that the ETKF has difficulty calibrating parameters when their influence on model outputs is strongly nonlinear. Bocquet and Sakov (2013) used the IEnKS for joint parameter and state estimation of the Lorenz-95 model and showed that the IEnKS outperforms other classical methods such as the Ensemble Kalman Filter, the Ensemble Kalman Smoother, and 4DVar. However, this study calibrated only two parameters. The main difference between these methods lies in whether an analytical solution is used (as in the Kalman Filter variants (Bishop et al., 2001; Peters et al., 2005)) or a gradient-based approach is adopted (as in the IEnKS (Bocquet and Sakov, 2014)). The original 4DEnVar method minimised the cost function using gradient computation (Liu et al., 2008; Liu and Xiao, 2013; Pinnington et al., 2020), but it

https://doi.org/10.5194/egusphere-2026-132
Preprint. Discussion started: 23 March 2026

can also employ an analytical solution under linearity assumptions (Douglas et al., 2025). More generally, there is still some debate about the appropriateness of its name.

The 4DEnVar method was first successfully applied to parameter estimation in a land surface model by Pinnington et al. (2020). In that study, seven crop parameters were calibrated in JULES using in situ observations of leaf area index, canopy height, and gross primary productivity (GPP) from the Mead site in Nebraska. The results demonstrated that 4DEnVar substantially reduced parameter uncertainty and improved the model's ability to reproduce observed vegetation dynamics, thereby highlighting the potential of the 4DEnVar method approaches for land surface model calibration without the need for an adjoint.

Subsequently, Douglas et al. (2025) examined the behaviour of 4DEnVar within a twin-experiment framework using a simple ecosystem carbon model, demonstrating its ability to recover model parameters while also highlighting sensitivities to ensemble size and configuration. Beylat et al. (2025) extended the application of 4DEnVar to the assimilation of atmospheric CO_2 concentration data in a twin-experiment setting, using ORCHIDEE coupled with the atmospheric transport model LMDZ. Their results showed that 4DEnVar could effectively handle computationaly expensive land-atmosphere coupling, leading to improved estimates of surface carbon fluxes.

In addition, 4DEnVar has been applied to improve soil moisture estimates in JULES. Cooper et al. (2021) showed that assimilating in situ soil moisture observations to optimise pedotransfer function parameters while Pinnington et al. (2021) assimilated satellite soil moisture data and Visweshwaran et al. (2025) assimilated in situ soil moisture observations for joint state–parameter calibration. All of these studies demonstrated improvements in JULES soil moisture estimates.

While the 4DEnVar DA technique has been successfully applied for land surface model calibration and has many apparent advantages, it must be exercised with caution. As we demonstrate in this study, when not set up with sufficient care, the method is capable of retrieving unlikely (out of an expected range) or even impossible (e.g. implausibly negative) parameter values, which can result in failed model runs using posterior parameters. This is due to a control variable transform of the original 4DVar cost function that it implements, affording the method limited restriction in its search for optimal and physically valid parameters (see section 2.2.3). In this article, we examine these behaviours and describe the key changes necessary to enable the assimilation of data that was not previously possible, giving special attention to the nuances of 4DEnVar. We illustrate the use of these adjustments in two complex land surface models: JULES and ORCHIDEE, the first calibration study of this nature to our knowledge. For JULES, we focus on a handful of directly related carbon parameters, whereas for ORCHIDEE, we consider a broader range of parameters, including some related to soil hydrology and phenology. By applying this method to two complex LSMs, we highlight the flexibility of the 4DEnVar method and its ability to tackle a varying number of parameters.

2 Models, Methods and Data

2.1 Land Surface Models and Parameter Selection

Many LSMs are currently in operational use; they vary in complexity and the number of inherent parameters and so their computational requirements differ. JULES and ORCHIDEE are examples of complex process-based land surface models that can be run at different spatial resolutions (ranging from site level to global). They can be used offline with meteorological

https://doi.org/10.5194/egusphere-2026-132
Preprint. Discussion started: 23 March 2026

forcing data (usually reanalyses such as the CRUJRA meteorological data (Kobayashi et al., 2015; Harris et al., 2020), as is done annually for the TRENDY model intercomparison exercise (Sitch et al., 2024)) or coupled to the atmosphere as part of an Earth System Model (ESM), for example, to contribute to the Coupled Model Intercomparison Project exercise (CMIP) (Williams et al., 2018; Boucher et al., 2020). LSMs also typically require other ancillary information, including fractions of land cover type in each grid cell, soil properties, atmospheric CO_2 concentration, and parameter values for the various incorporated submodels. Many of the parameters related to vegetative processes are specific to the plant functional types (PFTs) represented in the model, and each PFT requires a prescribed parameter value for each of these processes.

2.1.1 JULES

The JULES LSM is a community land surface model, the development of which is coordinated by the UK Met Office (UKMO) and the UK Centre for Ecology and Hydrology (UKCEH). JULES is the land surface component of the UKMO's Unified Model and is a key part of the UK's contribution to climate model intercomparison projects (e.g. CMIP7). The current version of JULES (at time of writing) is vn7.7 and is capable of modelling nine PFTs in standalone mode. As of version 5.6, JULES supports two options for modelling gross primary productivity (GPP), i.e. CO_2 assimilation during photosynthesis: 1) the Farquhar photosynthesis model (Farquhar et al., 1980), and 2) the Collatz photosynthesis model (Collatz et al. (1991), Collatz et al. (1992)). Additionally, as of version 7.5, JULES supports three options for modelling stomatal conductance: 1) the Jacobs model (Jacobs (1994); Best et al. (2011)), 2) the Medlyn model (Medlyn et al. (2011), Medlyn et al. (2012)), and 3) the SOX model (Eller et al., 2020). In this study, we select the Collatz and Medlyn models and calibrate a small subset of photosynthetic parameters (as opposed to the additional hydrological and phenological parameters selected for ORCHIDEE in Section 2.1.2). Table 1 shows the six photosynthetic parameters selected for JULES calibration following a sensitivity analysis using the methods of Morris (1991) and Campolongo et al. (2007).

2.1.2 ORCHIDEE

The ORCHIDEE (ORganizing Carbon and Hydrology In Dynamic EcosystEms, Krinner et al. (2005)) model is the land component of the IPSL Earth System Model (Boucher et al., 2020). ORCHIDEE separates processes according to their characteristic time scales. Rapid processes—including photosynthesis, surface energy exchanges, and hydrological fluxes—are simulated at a 30-minute resolution, whereas slower processes account for daily carbon allocation within vegetation, soil carbon cycling, and litter decomposition. Here we use ORCHIDEE version 2 in the configuration developed for the Coupled Model Intercomparison Project Phase 6 simulations (Boucher et al., 2020). Relative to the original version described by (Krinner et al., 2005), this release incorporates several developments, including revised schemes for soil hydrology, soil heat diffusion, soil organic matter dynamics, and plant photosynthesis. Photosynthesis is simulated as a function of incoming radiation, atmospheric CO_2, soil moisture availability, and near-surface air temperature. The calculations rely on the biochemical Farquhar–von Caemmerer–Berry model (Farquhar et al., 1980), following the formulation described by Yin and Struik (2009). Temperature responses of the parameters Vcmax and Jmax follow the approach proposed by Kattge and Knorr (2007). Soil hydraulic and thermal properties are determined from soil moisture and soil texture, with textures classified into 12 categories based on

https://doi.org/10.5194/egusphere-2026-132
Preprint. Discussion started: 23 March 2026

the USDA soil map (Reynolds et al., 2000). Vegetation is categorised into 14 Plant Functional Types (PFTs) based on shared structural and functional traits, plus one class for bare soil. For model calibration, we selected parameters critical for calculating GPP, as shown in Table 1. These parameters were chosen due to their importance in photosynthesis and their use (or that of their equivalents) in previous studies (Kuppel et al., 2012; Peylin et al., 2016; Bastrikov et al., 2018; Abadie et al., 2023).

Parameter name	**Description**	**Units**
JULES photosynthetic parameters		
α	Quantum efficiency of photosynthesis	mol CO_2 mol^{-1} PAR
n_e	Scale factor relating Vcmax with leaf nitrogen concentration	mol $CO_2 m^{-2} s^{-1}$ kg C (kg N)$^{-1}$
ω	Leaf scattering coefficient for PAR	N/A
T_{low}	Lower temperature threshold for photosynthesis	°C
T_{upp}	Upper temperature threshold for photosynthesis	°C
g_1	Sensitivity of stomatal conductance	$kPa^{0.5}$
ORCHIDEE		
Photosynthesis		
g_0	Residual stomatal conductance	$mol.m^{-2}.s^{-1}.bar^{-1}$
a_1	Empirical factor involved in the calculation of f_{VPD}	N/A
$Vc_{max_{25}}$	Maximum rate of Rubisco activity-limited carboxylation at 25°C	μ mol. $m^{-2}.s^{-1}$
$a_{r_{J,V}}$	Coeff. of linear regression defining Jmax25/Vcmax25 ratio	μ mol $.^{-1}\mu$ mol CO_2^{-1}
$a_{\Delta S,V}$	Coeff. of linear regression defining Entropy term for Vcmax	$J.K^{-1}.mol^{-1}$
$a_{\Delta S,J}$	Coeff. of linear regression defining Entropy term for Vcmax	$J.K^{-1}.mol^{-1}$
Phenology		
SLA	Specific leaf area	$m^2.gC^{-1}$
LAI_{max}	maximum LAI	$m^2.m^{-2}$
$c_{T_{crit}}$	Coefficient for critical temperature for senescence	K
$L_{age,crit}$	Critical leaf age	day
Hydrology		
Hum_{cst}	Constant of the exponential profile for root distribution	m
S	Scaling factor for soil resistance to evaporation	N/A

Table 1. JULES and ORCHIDEE parameters selected for optimisation with their descriptions and units.

2.2 The 4D Ensemble Variational (4DEnVar) Data Assimilation method

The 4DEnVar data assimilation method is derived from the classic 4DVar method (Courtier and Talagrand (1990), Rawlins et al. (2007)). In classic 4DVar, two probability distribution functions are assumed to be known: a prior (or background) distribution

https://doi.org/10.5194/egusphere-2026-132
Preprint. Discussion started: 23 March 2026

of the vector of target variables (state or parameters), and a likelihood distribution in space and time, which quantifies the probability of the observations given the target. A cost function with two corresponding quadratic terms is formulated from Bayesian inference under Gaussian assumptions of the aforementioned distributions, which balances the prior and observational information by their relative uncertainties. The inclusion of the prior term regularises the cost function and when linearised can be shown to be mathematically equivalent to Tikhonov regularisation (Freitag et al., 2010) (or ridge regression when concerning the magnitude of the solution) ensuring the existence of a unique, stabilised solution. However, minimisation of this cost function, to identify the optimised target vector, typically requires costly and burdensome tangent linear and adjoint derivations (which also require regular updates as the land surface models evolve), posing significant hurdles for implementation of the 4DVar method. Consequently, methods such as the 4DEnVar method have been developed to overcome this drawback.

The 4DEnVar method firstly implements a control variable transform to the cost function assuming that the true target value is a small perturbation to the prior knowledge of the target - much like incremental 4DVar (Courtier et al., 1994; Lorenc, 2003). Secondly, an ensemble of target vectors is generated to bypass the need for tangent linear and adjoint code by providing an approximation to gradient information. Posterior uncertainty information can be obtained from a posterior ensemble via an update to the original ensemble. In the context of parameter estimation, the target vectors are essentially the vectors of parameters to be optimised. Complex land surface models can include hundreds of parameters and so careful selection of a relevant subset may require a sensitivity analysis to identify the most important parameters prior to the use of 4DEnVar. Once a parameter subset is identified, their prior Gaussian distributions can be defined and a sample drawn according to the chosen ensemble size. This ensemble of parameters can then be passed to the model and outputs generated for comparison against the given observations.

2.2.1 Initial formulation

An ensemble of m parameter vectors of size n is drawn from a Gaussian distribution $\mathcal{N}(\mathbf{x}_b, \mathbf{B})$, where $\mathbf{x}_b$ denotes the expected value of the prior parameters and $\mathbf{B}$ its corresponding covariance matrix quantifying the uncertainty in the prior information. The mean of the parameter ensemble is found and denoted $\bar{\mathbf{x}}_b$. Subsequently, a matrix of parameter perturbation vectors is defined by:

$$\mathbf{X}'_{\mathrm{b}} = \frac{1}{\sqrt{m-1}} \left(\mathbf{X}_{b,1} - \overline{\mathbf{x}}_b, \mathbf{X}_{b,2} - \overline{\mathbf{x}}_b, \ldots, \mathbf{X}_{b,m} - \overline{\mathbf{x}}_b\right) \in \mathbb{R}^n \times \mathbb{R}^m, \tag{1}$$

where $\mathbf{X}_{b,i}$ $(i = 1, .., m)$ is an individual realisation of the parameter vector from the ensemble. Each of the ensemble members, as well as the ensemble mean, is mapped to observation space via the land surface model operator $\mathbf{h}$ and a perturbation matrix in observation space is defined:

$$\mathbf{Y}'_b = \frac{1}{\sqrt{m-1}} \left(\hat{\mathbf{h}}\left(\mathbf{X}_{\mathrm{b},1}\right) - \hat{\mathbf{h}}\left(\overline{\mathbf{x}}_{\mathrm{b}}\right), \ldots, \hat{\mathbf{h}}\left(\mathbf{X}_{\mathrm{b},m}\right) - \hat{\mathbf{h}}\left(\overline{\mathbf{x}}_{\mathrm{b}}\right)\right) \in \mathbb{R}^p \times \mathbb{R}^m, \tag{2}$$

where $\hat{}$ denotes concatenation of the simulated quantities and p is the total number of observations. An optimised parameter vector $\mathbf{x}^*$ is then determined by the control variable transform $\mathbf{x}^* = \bar{\mathbf{x}}_b + \mathbf{X}'_b \mathbf{w}^*$ (where $\mathbf{w}^*$ determines the optimal weightings of the ensemble parameter perturbations) and obtained via the minimisation of the following cost function (which uses

https://doi.org/10.5194/egusphere-2026-132
Preprint. Discussion started: 23 March 2026

$\mathbf{X}'_b(\mathbf{X}'_b)^T \approx \mathbf{B}$ and incorporates a linear Taylor expansion of $\hat{\mathbf{h}}(\bar{\mathbf{x}}_b + \mathbf{X}'_b\mathbf{w})$):

$$J(\mathbf{w}) = \frac{1}{2}\mathbf{w}^T\mathbf{w} + \frac{1}{2}\left(\hat{\mathbf{h}}(\bar{\mathbf{x}}_\mathrm{b}) + \mathbf{Y}'_b\mathbf{w} - \hat{\mathbf{y}}\right)^T \hat{\mathbf{R}}^{-1}\left(\hat{\mathbf{h}}(\bar{\mathbf{x}}_\mathrm{b}) + \mathbf{Y}'_b\mathbf{w} - \hat{\mathbf{y}}\right), \tag{3}$$

where $\hat{\mathbf{R}}$ is the observational error covariance matrix. A Taylor expansion of the forward model is used and $\mathbf{Y}'_b$ approximates gradient information - see Douglas et al. (2025) for more details. The cost function, now dependent on the weighting vector due to the control variable transform, is quadratic and can be analytically minimised, i.e. there is no need for the implementation of costly gradient-descent methods. By setting the corresponding gradient function to zero, the optimized weighting vector is given by:

$$\mathbf{w}^* = \left(\mathbf{I} + (\mathbf{Y}'_b)^T\hat{\mathbf{R}}^{-1}\mathbf{Y}'_b\right)^{-1}(\mathbf{Y}'_b)^T\hat{\mathbf{R}}^{-1}\left(\hat{\mathbf{y}} - \hat{\mathbf{h}}(\bar{\mathbf{x}}_\mathrm{b})\right). \tag{4}$$

The Hessian matrix of second derivatives of the cost function (3) in terms of control variables is $\mathbf{I} + (\mathbf{Y}'_b)^T\hat{\mathbf{R}}^{-1}\mathbf{Y}'_b \in \mathbb{R}^{n\times n}$, which is the inverse of the posterior error covariance matrix for $\mathbf{w}$. In this work, the square-root of this matrix in terms of parameters is found by first computing a matrix of scaled posterior perturbations $\mathbf{X}'_a$, which stems from the above Hessian calculation:

$$\mathbf{X}'_a = \mathbf{X}'_b\left(\mathbf{I} + (\mathbf{Y}'_b)^T\hat{\mathbf{R}}^{-1}\mathbf{Y}'_b\right)^{-\frac{1}{2}} \in \mathbb{R}^{n\times m}. \tag{5}$$

The posterior error covariance of the parameters is then $\mathbf{X}'_a(\mathbf{X}'_a)^T$ meaning that only knowledge of the $\mathbf{Y}'_b$ and $\hat{\mathbf{R}}$ matrices and prior knowledge of the parameters is required to complete the optimisation and quantify its associated uncertainty.

2.2.2 2D visualisations

We can visualize how the 4DEnVar method works for parameter calibration by considering a 2D case and using a simple function f that depends on two parameters a and b, as well as on a variable t, and that gives two outputs:

$$y_0 = f(t=0), \qquad y_1 = f(t=10). \tag{6}$$

We now consider two cases: one where f is linear with respect to a and b, denoted by f_1,

$$f_1(a,b) = a\cdot t + b, \tag{7}$$

and one where f is nonlinear with respect to a and b, denoted by f_2,

$$f_2(a,b) = \frac{a^2}{2}\cdot t + e^{\frac{b}{2}}. \tag{8}$$

In both cases, we define prior values $a=4$ and $b=3$, define a diagonal background error covariance matrix $\mathbf{B}$ with $\sigma_a = 0.5$ and $\sigma_b = 1$. Two sets of observations are generated using the functions f_1 and f_2 with $a=5$ and $b=5$, yielding $\boldsymbol{y}^{f_1}$ and $\boldsymbol{y}^{f_2}$. A random Gaussian noise $\mathcal{N}(0, 0.2)$ is then added to both synthetic observation sets. The observation error covariance matrix $\mathbf{R}$ is also diagonal, with a single standard deviation $\sigma = 0.2$. We can now calibrate the two parameters against the two observations

https://doi.org/10.5194/egusphere-2026-132
Preprint. Discussion started: 23 March 2026

$\boldsymbol{y}^{f_1}$ and $\boldsymbol{y}^{f_2}$ using the 4DEnVar method applied to each function f_1 and f_2. The same ensemble of 4 members is used in both cases.

Figure 1 shows the parameter space (left) as well as the model/observation spaces of both models f_1 (middle) and f_2 (right) at three different stages. The first stage (a) shows the prior value of the parameters and all ensemble members, together with their associated simulations using f_1 and f_2. The observations $\boldsymbol{y}^{f_1}$ and $\boldsymbol{y}^{f_2}$ are also shown, as well as the vectors in $\mathbf{X}'_b$ and $\mathbf{Y}'_{b_{1(2)}}$. The second stage (b) shows the same components, but the vectors $\mathbf{Y}'_b$, representing $\mathbf{f}_{1(2)}(\mathbf{X}_{\mathrm{b},i}) - \mathbf{f}_{1(2)}(\overline{\mathbf{x}}_{\mathrm{b}})$, are now multiplied by the corresponding weights w_i^* of the optimized weight vector $\mathbf{w}^*$. The third stage (c) shows the linear combinations $\mathbf{X}'_b\mathbf{w}^*_{1(2)}$ and $\mathbf{Y}'_{b_{1(2)}}\mathbf{w}^*_{1(2)}$. The red dot represents the posterior parameter value and its associated simulation for the case using f_1, while the purple dot represents the same for the case using f_2. The crosses in the model/observation spaces correspond to $\mathbf{f}_{1(2)}(\overline{\mathbf{x}}_{\mathrm{b}}) + \mathbf{Y}'_{b_{1(2)}}\mathbf{w}^*_{1(2)}$.

Let us first consider the linear model f_1 assimilating $\boldsymbol{y}^{f_1}$. The model is linear in a and b. Therefore, the linear combination in $\mathbf{Y}'_{b_1}\mathbf{w}^*_1$ can closely mimic the model itself. This linear combination can be optimised to reduce the distance between the prior simulation and the observation $\boldsymbol{y}^{f_1}$, and it can be used in parameter space to find the true parameters that generated the observation. When applying model f_1 to the posterior parameters, the resulting simulation matches the result obtained from the linear combination. In the second case, using f_2 and assimilating $\boldsymbol{y}^{f_2}$, the model is no longer linear in a and b. Therefore, the optimised linear combination cannot mimic the model, and the posterior parameters obtained do not recover the true parameter values. We also observe a large discrepancy in observation space between the linear combination $\mathbf{f}_2(\overline{\mathbf{x}}_{\mathrm{b}}) + \mathbf{Y}'_{b_2}\mathbf{w}^*_2$ and the true model output $\mathbf{f}_2(\mathbf{x}_{\mathrm{a}})$.

These two simple cases help illustrate how the method works and provide insight into its behaviour. In both cases, the optimised linear combination recovers the observation point; however, in the second case, this linear combination cannot replicate the nonlinear model f_2. This introduces a bias between $\mathbf{f}_2(\overline{\mathbf{x}}_{\mathrm{b}}) + \mathbf{Y}'_{b_2}\mathbf{w}^*_2$ and $\mathbf{f}_2(\mathbf{x}_{\mathrm{a}})$, and prevents recovery of the correct parameter values. This illustrates one of the limitations of using the 4DEnVar method and shows the necessity of implementing an alternative approach such as including a regularisation term to handle situations where the model is not linear. A similar issue can arise even with a linear model: if the variability of assimilated observations cannot be reached by the model, and this information is not properly represented in the matrix $\mathbf{R}$, the method may behave in the same way.

2.2.3 Regularised optimisation

The 4DEnVar method relies on a linearity assumption introduced by the use of the weighting vector and the Taylor expansion of the forward model. This has the advantage of circumventing the need for tangent linear and adjoint codes but may not respect physical laws in the way that gradient information from an explicitly differentiated version of the model does. In addition, as with 4DVar, it is possible that a large observational cost term (e.g. when too many observations are implemented or observation errors are too small) renders the background term almost negligible and effectively loses all prior knowledge. In the case of 4DEnVar, due to the control variable transform, optimal weights will prioritise a match between the ensemble and observations in observation space which, when applied in parameter space, can lead to implausible (out-of-bounds) or non-physical (e.g., negative) parameter values. Even when the obtained parameter vector seems plausible, applying the model operator can still

https://doi.org/10.5194/egusphere-2026-132
Preprint. Discussion started: 23 March 2026

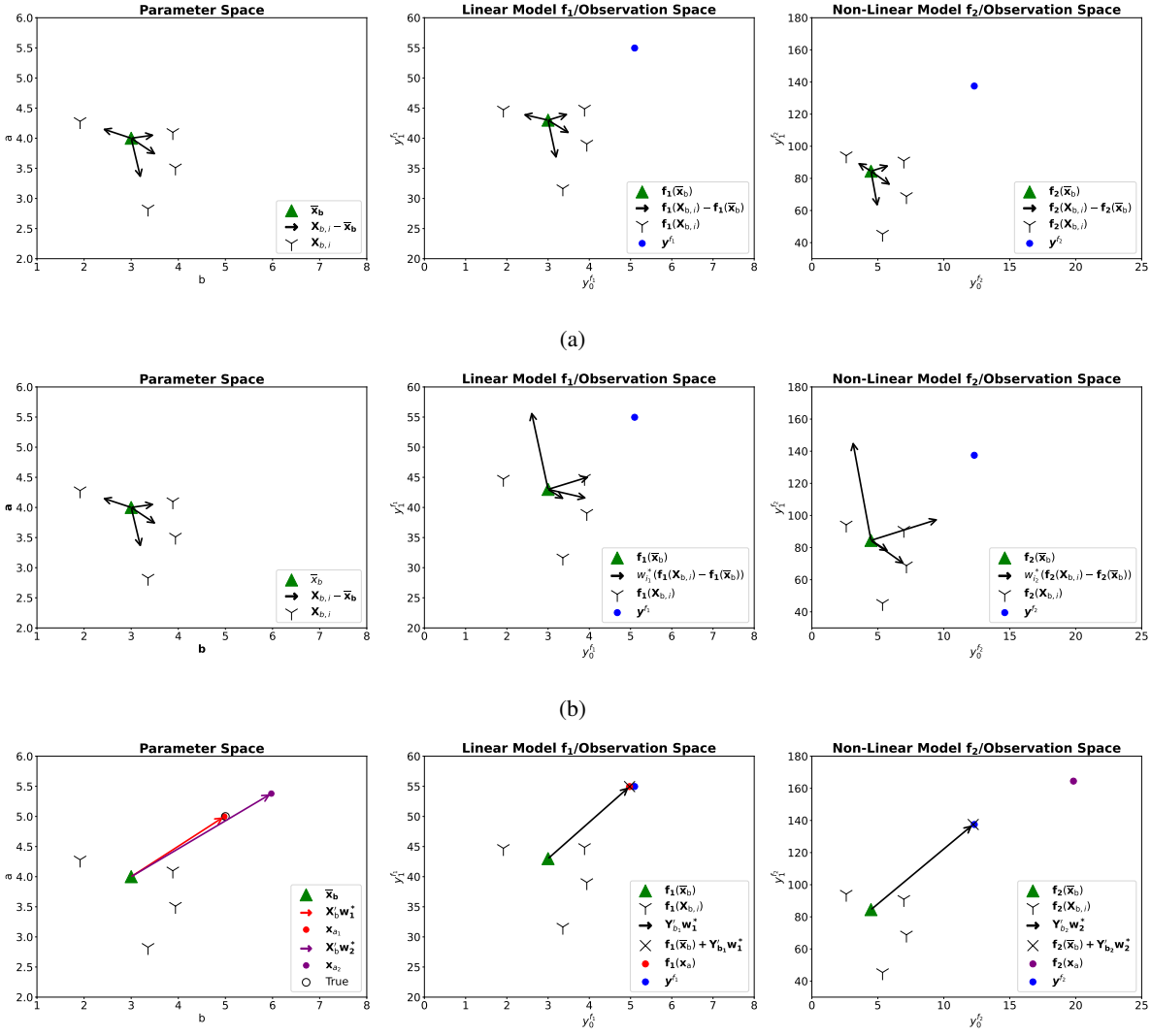

Figure 1. Visualisation of the 4DEnVar method across three successive stages applied to a linear and non-linear model. The left panels represent the parameter space, while the middle and right panels show the model and observation spaces corresponding to the models f_1 (the linear model) and f_2 (the non-linear model), respectively. In the first stage (a, top), the prior parameter value (green triangle) and all ensemble members (black triangles) are displayed, together with their associated simulations produced by f_1 and f_2. The observations (in blue), $\boldsymbol{y}^{f_1}$ and $\boldsymbol{y}^{f_2}$, are also shown, along with the vectors in $\mathbf{X}'_b$ and $\mathbf{Y}'_{b_{1(2)}}$ (black arrows). The second stage (b, middle) presents the same elements; however, the vectors $\mathbf{Y}'_b$, defined as $\mathbf{f}_{1(2)}(\mathbf{X}_{\mathrm{b},i}) - \mathbf{f}_{1(2)}(\overline{\mathbf{x}}_\mathrm{b})$, are now scaled by the corresponding weights w_i^* from the optimised weight vector $\mathbf{w}^*$. The third stage (c, bottom) shows the resulting linear combinations $\mathbf{X}'_b\mathbf{w}^*_{1(2)}$ (in red for f_1 and in purple for f_2) and $\mathbf{Y}'_{b_{1(2)}}\mathbf{w}^*_{1(2)}$ (in black). The red marker denotes the posterior parameter estimate and its associated simulation for model f_1, while the purple marker denotes the corresponding posterior estimate for model f_2. The crosses in the model/observation spaces represent the quantities $\mathbf{f}_{1(2)}(\overline{\mathbf{x}}_\mathrm{b}) + \mathbf{Y}'_{b_{1(2)}}\mathbf{w}^*_{1(2)}$. The circle represent the True parameter that was used to generated the observations $\boldsymbol{y}^{f_1}$ and $\boldsymbol{y}^{f_2}$

https://doi.org/10.5194/egusphere-2026-132
Preprint. Discussion started: 23 March 2026

degrade the data fit, due to non-compliance with the physical laws represented in individual model runs. In order to overcome this issue, a hyperparameter, γ, can be applied to the background term so that the cost function becomes:

$$J(\mathbf{w}) = \frac{1}{2}\gamma\mathbf{w}^T\mathbf{w} + \frac{1}{2}\left(\hat{\mathbf{h}}\left(\overline{\mathbf{x}}_\mathrm{b}\right) + \mathbf{Y}_b'\mathbf{w} - \hat{\mathbf{y}}\right)^T \hat{\mathbf{R}}^{-1}\left(\hat{\mathbf{h}}\left(\overline{\mathbf{x}}_\mathrm{b}\right) + \mathbf{Y}_b'\mathbf{w} - \hat{\mathbf{y}}\right). \tag{9}$$

This factor (often called the ridge parameter), when greater than 1, simply increases the background term so that the optimised parameter vector $\mathbf{x}^*$ will be (by construction) closer to the prior parameter vector $\mathbf{x}_b$ and goes some way to maintain the validity of the linear assumption during the minimisation process. This factor is incorporated into the optimisation of the optimal weighting vector as follows:

$$\mathbf{w}^* = \left(\gamma\mathbf{I} + \left(\mathbf{Y}_b'\right)^T\hat{\mathbf{R}}^{-1}\mathbf{Y}_b'\right)^{-1}\left(\mathbf{Y}_b'\right)^T\hat{\mathbf{R}}^{-1}\left(\hat{\mathbf{y}} - \hat{\mathbf{h}}\left(\overline{\mathbf{x}}_\mathrm{b}\right)\right), \tag{10}$$

(essentially equivalent to a ridge regression) as well as the posterior error covariance matrix found from $\mathbf{X}_a'(\mathbf{X}_a')^T$:

$$\mathbf{X}_a' = \mathbf{X}_b'\left(\gamma\mathbf{I} + \left(\mathbf{Y}_b'\right)^T\mathbf{R}^{-1}\mathbf{Y}_b'\right)^{-\frac{1}{2}}. \tag{11}$$

While a γ value (or ridge parameter) greater than one gives additional weighting to the background term, it should be noted that a γ value too small (large) will result in overfitting (underfitting) the observations. Several methods exist for the selection of γ that attempt to address this trade-off, in an optimal way, that vary from arbitrary/empirical selection to fully statistical approaches. Example methods include the L-curve criterion (Hansen, 1992), Generalised Cross Validation (Golub et al., 1979), and the Morozov discrepancy principle (Morozov, 1984). The L-curve criterion approach considers the prior norm ($||\mathbf{x}^* - \mathbf{x}_b||_2$) plotted against the residual norm ($||\mathbf{y} - h(\mathbf{x}^*)||_2$) for a range of ridge parameter values with the "corner" (or "knee") representing the optimal trade-off minimising overfitting without excessive damping of the solution. Generalised cross validation selects the ridge parameter that minimises the ratio of the residual norm and complexity penalty for a model, while the Morozov discrepancy principle is based on finding the regularisation parameter such that the posterior observational errors are consistent with the expected level of observational noise. Furthermore, it is possible to locate a γ that ensures an analysis that is statistically consistent with both the prior and observations using, for example, Desrozier's consistency diagnostics (Desroziers et al., 2005). While variations of these methods have been applied in numerical weather prediction (Xu et al. (2006); Gratton et al. (2007)), to our knowledge, they have not been applied in an LSM setting. To translate these methods to the case of 4DEnVar, via the control variable transform, one can quantify the prior norm as $||\mathbf{w}^*||_2 = \sqrt{\mathbf{w}^{*T}\mathbf{w}^*}$ and the residual norm as $||\hat{\mathbf{h}}\left(\overline{\mathbf{x}}_\mathrm{b}\right) + \mathbf{Y}_b'\mathbf{w}^* - \hat{\mathbf{y}}||_2 = \sqrt{\left(\hat{\mathbf{h}}\left(\overline{\mathbf{x}}_\mathrm{b}\right) + \mathbf{Y}_b'\mathbf{w}^* - \hat{\mathbf{y}}\right)^T\left(\hat{\mathbf{h}}\left(\overline{\mathbf{x}}_\mathrm{b}\right) + \mathbf{Y}_b'\mathbf{w}^* - \hat{\mathbf{y}}\right)}$. However, we note that $\hat{\mathbf{h}}\left(\overline{\mathbf{x}}_\mathrm{b}\right) + \mathbf{Y}_b'\mathbf{w}^*$ serves as a linear approximation to $\hat{\mathbf{h}}\left(\mathbf{x}^*\right)$ and so these norms are calculated without the need for posterior model runs. Consequently, any γ chosen this way does not translate well to the calculation of genuine posterior residual norms. As an example to illustrate this point, one can simply consider the case where $\gamma = 1$ that results in implausible parameter values - the residual norm can be calculated in $\mathbf{w}$-space but it is not possible to calculate the true residual norm as the model can not be run on the corresponding parameters in $\mathbf{x}$-space. A deterioration of the L-curve, when plotting the prior norm against the residual norm using the linear approximation versus using the posterior model run, can be seen in Appendix A.

https://doi.org/10.5194/egusphere-2026-132
Preprint. Discussion started: 23 March 2026

In this study, we circumvent the inability to apply standard γ selection techniques by choosing the value of γ that minimises the RMSE in the posterior model run while providing physically realistic posterior parameters. This choice is used to illustrate the potential of the 4DEnVar method to provide the best fit to observations for two complex land surface models.

2.3 Experiment

To demonstrate the 4DEnVar method's effectiveness and versatility, we applied the technique to two distinct test cases: i) to the JULES LSM with a focused set of 6 GPP-related parameters, and ii) to the ORCHIDEE LSM with a broader range of 12 parameters including soil hydrology and phenology. This approach illustrates 4DEnVar's capacity to handle different model structures and parameter spaces. Both models are run offline at the Harvard Forest site (FLUXNET2015 Dataset, 2015) using the meteorological forcing data provided by the FluxNet network for this site (Pastorello et al., 2020). For both models, we assimilate GPP observations derived from Net Ecosystem Exchange eddy covariance tower measurements. The assimilation period covers the years 1992 to 2009 where the monthly average of the observations are assimilated and compared against the monthly average of the simulations.

The prior parameters for the JULES LSM are in Table B1. The model was spun-up over the years where FluxNet data was available (1992-2012) and repeated over 3 cycles. This was sufficient to spinup the variables controlling the short term variability of GPP.

Given that the ORCHIDEE LSM was previously extensively optimised using these observations, its default parameters already show excellent agreement with the FluxNet data. To properly evaluate the method's performance with ORCHIDEE, we generated a new set of a priori parameters using uniform distributions bounded by physically plausible values shown in Table B1. The ORCHIDEE LSM carbon pools are brought to equilibrium using a full TRENDY spin-up (Sitch et al., 2024) including:

- A spin-up simulation of 200 years recycling FluxNet meteorological data with atmospheric CO_2 concentration fixed at its pre-industrial value of 1700;
- A transient simulation recycling FluxNet meteorological data with variations in atmospheric CO_2 concentration between 1700 and 1992.

The 4DEnVar parameter ensembles consisted of 20 members for the JULES LSM and 100 members for the ORCHIDEE LSM, as a larger number of parameters were calibrated for ORCHIDEE. The respective parameter ensembles were then passed to their models for the generation of model trajectories forming the ensembles in observation space. Once generated, the same observations for both models are used to perform different assimilation experiments with different γ values and a fixed diagonal $\mathbf{R}$-matrix with standard deviation of 0.35 (gC m^{-2} d^{-1}) for both LSMs representing the joint model-observation error. The ensemble of a posteriori parameters for each experiment is then used to perform the a posteriori simulation, and the best performance in terms of RMSE is retained to present the optimal analysis - see Figure 2. The simulation is extended to the year 2012 - the latest available year of observations in the FLUXNET2015 dataset used - in order to validate the posterior model runs over the years 2010-2012 (not used for the calibration).

https://doi.org/10.5194/egusphere-2026-132
Preprint. Discussion started: 23 March 2026

3 Results

3.1 Influence of the γ-hyperparameter

Figure 2 shows the influence of the γ value on the posterior (prior) RMSE computed between the monthly mean observations and the monthly mean post-optimisation (pre-optimisation) simulations for increasing γ values (γ does not affect the prior RMSE). The prior RMSE for the JULES LSM is 5.06 gC m^{-2} d^{-1}, whereas the prior RMSE for the ORCHIDEE LSM is 2.61 gC m^{-2} d^{-1}. Note that in the case of JULES, the curve begins at a higher value of γ; this is where values of γ start to produce feasible parameter values for posterior JULES runs. Values for γ were:

$$\text{JULES:} \quad [30, 40, 50, 60, 70, 80, 90, 100, 150, 200, 2000, 10000, 100000, 1000000, 10000000]$$

$$\text{ORCHIDEE:} \quad [1, 10, 100, 1000, 10000, 100000]$$

Both curves show a reduction in posterior RMSE with increasing γ values reaching a minimum at the optimal γ value, increasing again as we further increase γ and converging to the prior RMSE. The minimum posterior RMSE obtained for the JULES LSM is 1.15 gC m^{-2} d^{-1} with a γ value of 60, while the minimum posterior RMSE obtained for the ORCHIDEE LSM is 1.12 gC m^{-2} d^{-1} with a γ value of 100.

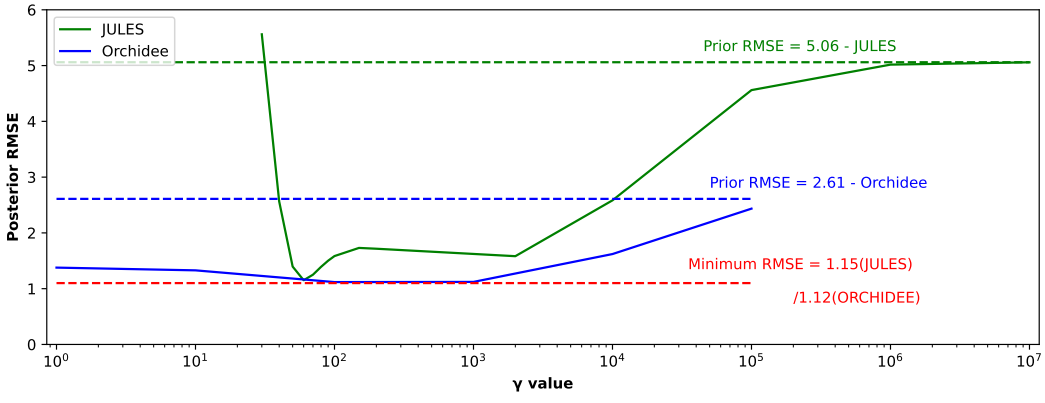

Figure 2. Posterior RMSE quantifying the difference between posterior model runs and observations for increasing γ values for both JULES and ORCHIDEE LSMs.

3.2 Results of the calibration

In Figure 3, we show the parameter ensemble means and standard deviations of the prior ensemble (in green) and two posterior ensembles: one computed using the optimal γ value (in red) found in Section 3.1 and one without tailored regularisation, i.e. $\gamma = 1$ (in blue). Figure 3a presents the results for the JULES LSM parameters, while Figure 3b shows those for the ORCHIDEE LSM parameters. We observe significant differences between the means and standard deviations between the

https://doi.org/10.5194/egusphere-2026-132
Preprint. Discussion started: 23 March 2026

posterior parameter ensembles for both models. Most notably, several parameter means obtained from standard optimisations
305 ($\gamma = 1$) fall outside their prescribed ranges: n_{eff} and t_{upp} for the JULES LSM, and $\mathbf{Vc_{max_{25}}}$ for the ORCHIDEE LSM. Some of the ORCHIDEE means also shift in different directions, most noticeably in $\mathbf{a_{\Delta S,V}}$. Additionally, the standard deviations of the posterior ensembles obtained using the optimal γ value are consistently narrow for all parameters in both models.

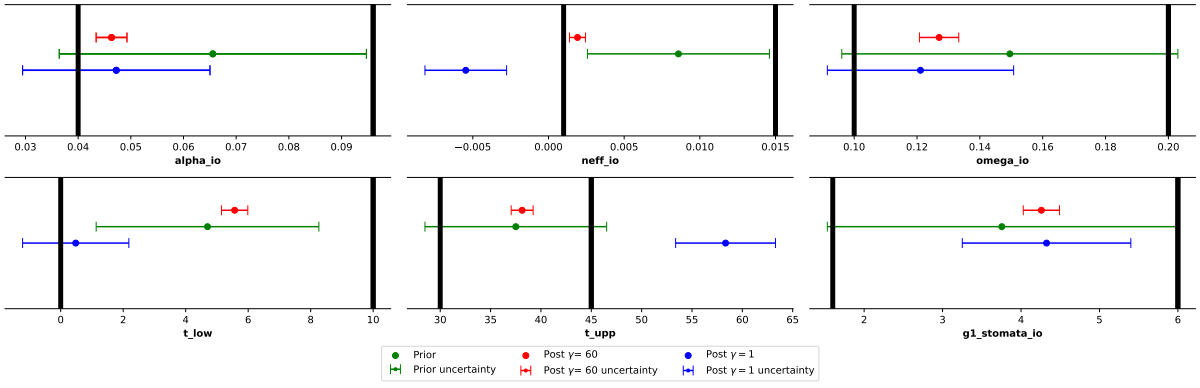

(a) JULES prior and posterior parameter distributions.

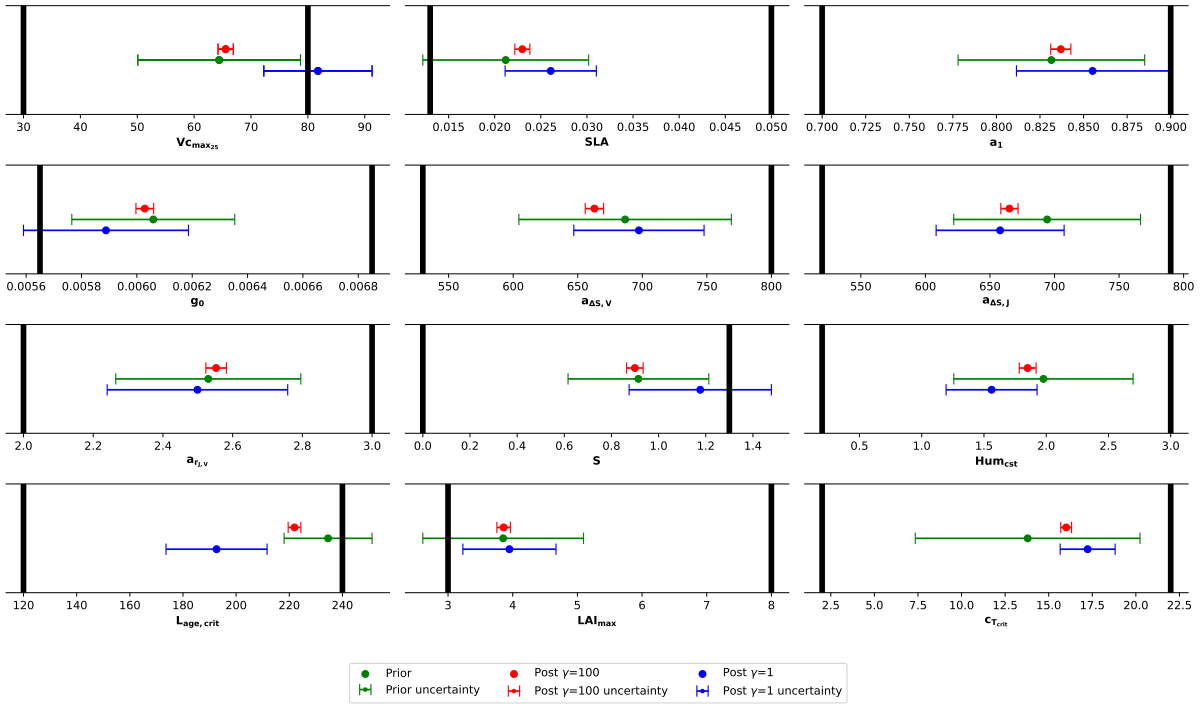

(b) ORCHIDEE prior and posterior parameter distributions.

Figure 3. Prior and posterior parameters in the $\gamma = 1$ and $\gamma > 1$ optimisations for both JULES (top panel) and ORCHIDEE (bottom panel) experiments. Black vertical bars represent prior parameter bounds.

https://doi.org/10.5194/egusphere-2026-132
Preprint. Discussion started: 23 March 2026

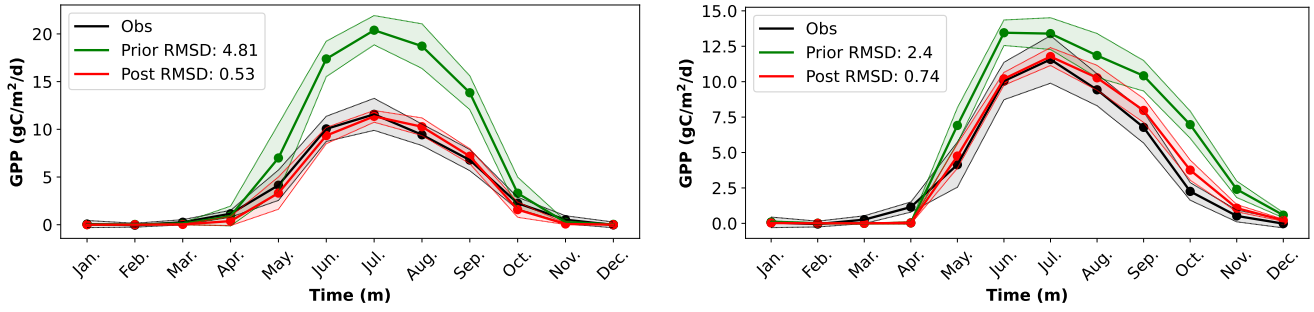

(a) JULES prior and posterior GPP against observations annually averaged over the years 1992-2012.

(b) ORCHIDEE prior and posterior GPP against observations annually averaged over the years 1992-2012.

Figure 4. Prior and posterior outputs of GPP for JULES (left panel) and ORCHIDEE (right panels) experiments.

Figure 4 shows the mean and standard deviation of the seasonal cycle of GPP for the observations (in black), prior simulation (in green), and posterior simulation using the optimal γ (in red). The RMSE values are computed between the mean seasonal cycle of the observations and each of the simulations. The prior RMSE values are 4.81 gC m^{-2} d^{-1} and 2.4 gC m^{-2} d^{-1} for JULES and ORCHIDEE LSMs respectively, decreasing to 0.53 gC m^{-2} d^{-1} and 0.74 gC m^{-2} d^{-1} in the posterior simulations. For the JULES LSM, the prior simulation shows significant overestimation of GPP compared to observations across active months. The posterior simulation demonstrates good fit to observations with only slight underestimation during spring. Regarding the ORCHIDEE LSM, the prior simulation overestimates GPP from April to the end of the year although this overestimation is much smaller in magnitude in comparison to the JULES prior. The ORCHIDEE posterior simulation also shows good agreement with observations, with only a slight overestimation of GPP during autumn and a late onset of active GPP in May (by one month).

3.3 Results in validation period

Figure 5 shows the monthly GPP time series for observations and posterior simulations of both JULES and ORCHIDEE LSMs using their respective optimal γ values during the validation period (2010-2012). The RMSE values between observations and simulations are 1.63 gC m^{-2} d^{-1} and 1.92 gC m^{-2} d^{-1} for JULES and ORCHIDEE LSMs respectively, with both models showing slight underestimation of GPP. Notably, the 2010 observations exhibit a monthly maximum GPP that is offset by one month compared to the simulations from both models. In this case, the models have been calibrated with observations where GPP peaks are happening in July. In 2010, however, whether down to observational error, changes in meteorological forcing data or a genuine early peak in photosynthesis, the models are unable to reach this peak seen in observations when run with the optimised parameter values.

https://doi.org/10.5194/egusphere-2026-132
Preprint. Discussion started: 23 March 2026

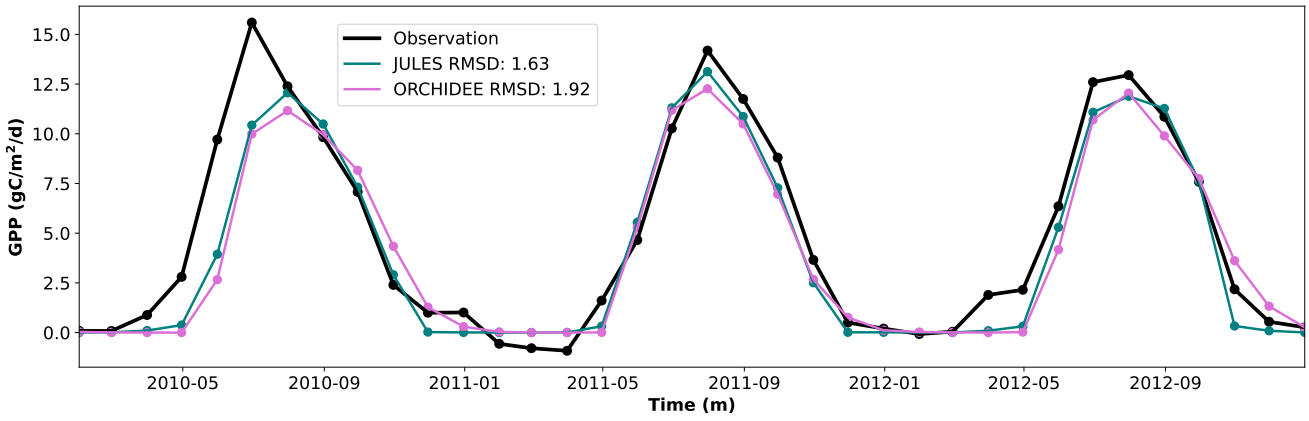

Figure 5. Posterior JULES and ORDHIDEE model runs using respective optimised parameters optimal γ values for each month (m) in the validation years 2010-2012.

4 Discussion

The results show that the 4DEnVar data assimilation method, in the context of parameter estimation for land surface modelling, is versatile and works effectively with the caveat that, when used with real observations (or indeed any case when the variability in the observations is not well captured by the model), the method must be exercised with caution. The control variable transform of the classic 4DVar function, while circumventing the need for tangent linear and adjoint calculations, introduces a flexibility that can result in locating infeasible parameters in the optimisation. When implementing tailored regularisation through the incorporation of the γ hyperparameter, the method is able to locate parameters that produce posterior runs that match observations well, even into the validation period, for both the JULES model (where a handful of photosynthetic parameters are selected and a relatively small ensemble size) and the ORCHIDEE model (where a larger subset of parameters and a larger ensemble size are selected). In both cases, the optimised parameter sets are identified with narrow distributions compared to optimisations with γ fixed at 1 (i.e. original 4DEnVar cost function), indicating that a γ value different from 1 may improve parameter calibration exercises in land surface modelling.

The selection of the γ value to use in the optimisation remains a challenge. Typical techniques in data assimilation that seek to optimise the trade off between prior information and observations are not applicable in the case of 4DEnVar. However, by sampling over γ values, we were able to identify approximate values of γ for both models that gave the lowest RMSE in posterior models runs against observations. This technique would not be practical in multiple site settings or global optimisations as it detracts from the efficiency of the 4DEnVar method. Further studies should explore techniques that identify γ without the need for posterior model runs, such as restriction of the magnitude of the weighting vector to maintain compliance with linearity assumptions. However, a single optimal value for γ may not be necessary; a range of γ values facilitates successful optimisation

https://doi.org/10.5194/egusphere-2026-132
Preprint. Discussion started: 23 March 2026

against real observations (where $\gamma = 1$ fails), leading to reduced RMSE between posterior simulations and observations, as seen in Figure 2, not necessarily minimised.

The 4DEnVar method offers significant advantages over current operational data assimilation methods, most notably but not limited to, the avoidance of complex tangent linear and adjoint code construction and maintenance. Following the generation of an ensemble of model runs, the analysis step of the method is fast and modification of the model code is not required. For a fixed γ (or indeed γ that is not determined by posterior model runs), this ensemble can also then be used in further experiments, such as against different observations or with redefined $\mathbf{R}$-matrix (observation error covariance matrix) without the need for completing additional model runs (except the posterior model run once parameters have been optimised).

Note that 4DEnVar can be implemented effectively across different modelling environments, whether or not a formal calibration framework is available. This highlights its practical flexibility: it can be applied with relative ease in models that have not yet undergone extensive calibration, while also integrating naturally into existing structured frameworks. Specifically, the ORCHIDEE model benefits from the ORCHIDAS framework, which provides a formal calibration structure and robust parameter constraints. While ORCHIDEE has previously been calibrated against FluxNet observations within this framework, our results in this paper show that the 4DEnVar method can also be used to reduce the RMSE in posterior simulations, with potential for additional gains from a more extensive search in γ space (albeit with greater computational expense). In contrast, although JULES does not yet have a comparable framework, we demonstrate that 4DEnVar can still be applied just as effectively, underlining its adaptability and value across a range of modelling contexts.

It should be noted that, while γ adjusts the weight of the prior term in the 4DEnVar cost function, the same effect can be achieved by tuning the $\mathbf{R}$-matrix which determines the weight of the observational cost term. The selection of γ is therefore intrinsically linked to the characterisation of the $\mathbf{R}$-matrix. Increasing the uncertainty in this matrix effectively reduces the weight assigned to the observational terms, thereby increasing the relative influence of the background terms. However, $\mathbf{R}$ incorporates both observation errors and model-related errors. While observation errors can, in principle, be prescribed, obtaining a reliable quantification of model errors remains a complex and challenging task. Consequently, the parameter γ may also be adjusted to compensate for inaccuracies in the specification of $\mathbf{R}$, effectively increasing the weight of the observations when the error statistics are poorly estimated.

As land surface community interest in the 4DEnVar method increases, practitioners should be aware of the potential need for the γ adjustment in the cost function and previous studies where analyses have been performed entirely in a twin experimental setting, such as Beylat et al. (2025), can be revisited to exploit this technique.

5 Conclusion

The 4DEnVar data assimilation method can be implemented to calibrate land surface models in order to reduce the RMSE between model simulations and observed measurements. In this study, we calibrated two land surface models, JULES and ORCHIDEE, against FluxNet measurements of GPP at the Harvard site, resulting in comparable RMSEs in the posterior model runs. As well as the versatility in terms of ensemble size, parameter set selection and choice of land surface model, the

https://doi.org/10.5194/egusphere-2026-132
Preprint. Discussion started: 23 March 2026

4DEnVar method also benefits from speed and ease of use and its avoidance of using tangent linear and adjoint calculations. However, the method has potential to fail when implemented without tailored regularisation, due to the introduction of the control variable transform, and it may be essential to implement the γ-hyperparameter into the cost function to regulate this drawback. Traditional techniques for γ selection do not apply here and so further work that fully exploits the low computational expense of the method is required. Nevertheless, the regularised adaptation through the use of γ offers potential to those in land surface model calibration wishing to move from a twin experiment setting in favour of utilising real observations.

Appendix A: L-curves

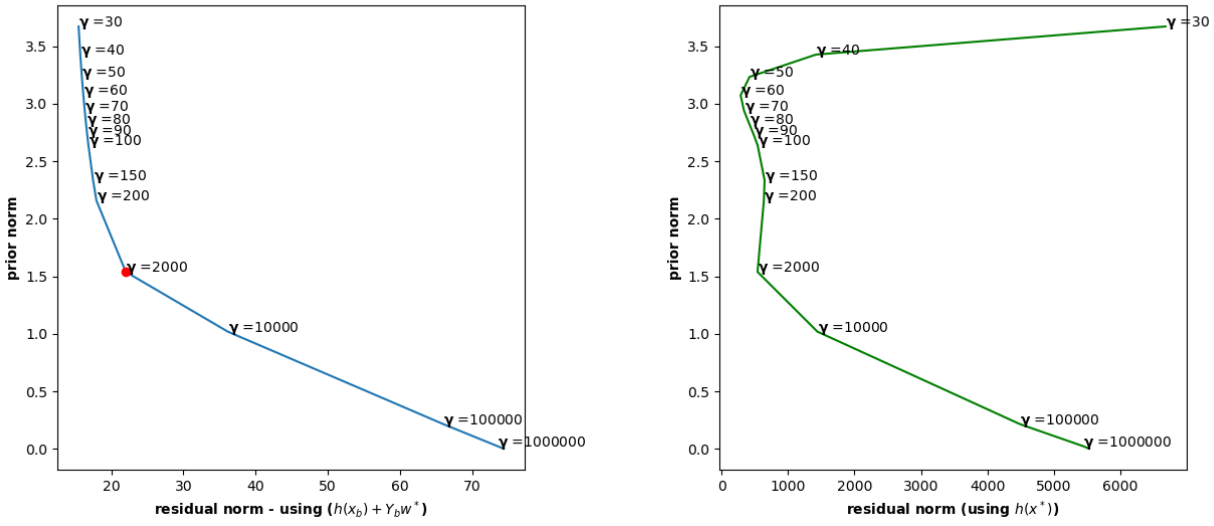

(a) Prior versus posterior residual norms using the linear approximation.

(b) Prior versus posterior residual norms using posterior model runs.

Figure A1. Prior versus posterior residual norms when using the linear approximation (left) in the observational cost term and using the posterior model run (right). The JULES experiment was used to generate the plots and we see that standard techniques (such as the L-curve) cannot be used to select γ when applying 4DEnVar.

Appendix B: JULES parameters

Table B1 shows the prior information on the JULES parameters that were calibrated in this study, including the lower and upper bounds set for sampling. The means for each parameter are calculated post sampling from the multivariate Normal distribution $\mathcal{N}(\mathbf{x}_b, \mathbf{B})$ where $\mathbf{x}_b$ is the vector of prior parameter values and $\mathbf{B}$ is the diagonal matrix of variances with standard deviation set to 0.5 times the prior parameter value. Parameter samples were discarded if they fell outside the given ranges and resampled until the ensemble size of 20 was reached. Two optimisations are performed: one where there is no restriction on the cost

https://doi.org/10.5194/egusphere-2026-132
Preprint. Discussion started: 23 March 2026

function ($\gamma = 1$) and a second optimisation where an optimised factor ($\gamma = 60$) is placed on the prior term in the cost function. This value is chosen following the analysis of Figure 2 and gives more weight to the prior term so that infeasible parameters, such as a negative n_{eff}, are not obtained in the optimisation.

Parameter	Prior	LB	UB	UA	OA
JULES					
α	0.068	0.04	0.096	0.04724	0.04675
n_e	0.008	0.001	0.015	-0.0005465	0.001409
ω	0.15	0.1	0.2	0.1211	0.1262
T_{low}	5.0	0.0	10.0	0.4808	5.5402
T_{upp}	37.5	30.0	45.0	58.3362	38.2880
g_s	3.8	1.6	6.0	4.3259	4.2707
ORCHIDEE					
g_0	0.00605	0.00685	0.00685	0.00589	0.00603
a_1	0.83	0.7	0.9	0.86	0.84
$Vc_{max_{25}}$	64	30	80	82	66
$a_{r_{J,V}}$	2.53	2	3	2.50	2.55
$a_{\Delta S,V}$	686	530	800	697	662
$a_{\Delta S,J}$	694	520	790	657	665
SLA	0.021	0.013	0.05	0.026	0.023
LAI_{max}	3.9	3	8	3.9	3.9
$c_{T_{crit}}$	14	2	22	17	16
$L_{age,crit}$	234	120	240	192	221
Hum_{cst}	1.98	0.2	3	1.56	1.85
S	0.91	0	1.3	1.17	0.90

Table B1. Prior values (Prior), lower bounds (LB), upper bounds (UB), the values obtained from analysis with $\gamma = 1$ (UA) and analysis with optimal γ (OA) using $\gamma = 60$ for the JULES parameters and $\gamma = 100$ for the ORCHIDEE parameters selected for experimentation.

https://doi.org/10.5194/egusphere-2026-132
Preprint. Discussion started: 23 March 2026

Code and data availability

All model code, detailed notes on the derivation of the 4DEnVar method, and scripts used for figure generation and output processing are archived on Zenodo: https://doi.org/10.5281/zenodo.19001565 Douglas (2026). The archived version corresponds to the GitHub repository available at: https://github.com/NatalieDouglas/4DEnVar.

All JULES model runs can be repeated and results replicated using the `u-dr501` suite accessible at the Met Office Science Repository Service (https://code.metoffice.gov.uk, last access: March 2026, login required). This suite is an adaption of the widely used and continually developed `u-al752` Fluxnet suite (Harper et al. (2021)).

The implementation of the ORCHIDEE model used in this study is openly accessible and can be obtained via the following DOI: https://doi.org/10.14768/c68bc728-da71-4383-84df-dcde31d9c006 ORCHIDEE (2025). The work ORCHIDAS EnVarDA used in this work is archived in a Zenodo repository and available at https://doi.org/10.5281/zenodo.14609416 Beylat (2025).

Meteorological forcing data for the US-Ha site are provided by the FLUXNET2015 dataset and can be accessed online once users have registered https://fluxnet.org/data/fluxnet2015-dataset/ (Pastorello et al., 2020)

Author contributions

ND, SB and NR conceived on the study. ND performed the DA experiments using JULES. SB performed the DA experiments using ORCHIDEE. ND and SB analysed the results. TQ, PP and NR provided expertise on parameter calibration. RB provided expertise on DA methods. ND and SB wrote the article. All the co-authors reviewed and edited the article.

Competing Interests

The authors declare that no competing interests are present

Acknowledgements

Natalie Douglas has been supported by the UKRI National Centre for Earth Observation, under the International Science Programme (NE/X006328/1). Simon Beylat has been supported by a scholarship from CNRS under the Melbourne–CNRS joint doctoral programme.

https://doi.org/10.5194/egusphere-2026-132
Preprint. Discussion started: 23 March 2026

References

Abadie, C., Maignan, F., Remaud, M., Kohonen, K.-M., Sun, W., Kooijmans, L., Vesala, T., Seibt, U., Raoult, N., Bastrikov, V., Belviso, S., and Peylin, P.: Carbon and water fluxes of the boreal evergreen needleleaf forest biome constrained by assimilating ecosystem carbonyl sulfide flux observations, Journal of Geophysical Research, 128, https://doi.org/10.1029/2023jg007407, 2023.

Bacour, C., Peylin, P., MacBean, N., Rayner, P. J., Delage, F., Chevallier, F., Weiss, M., Demarty, J., Santaren, D., Baret, F., Berveiller, D., Dufrêne, E., and Prunet, P.: Joint assimilation of eddy covariance flux measurements and FAPAR products over temperate forests within a process-oriented biosphere model, Journal of Geophysical Research: Biogeosciences, 120, 1839–1857, https://doi.org/https://doi.org/10.1002/2015JG002966, 2015.

Bastrikov, V., MacBean, N., Bacour, C., Santaren, D., Kuppel, S., and Peylin, P.: Land surface model parameter optimisation using in situ flux data: Comparison of gradient-based versus random search algorithms (a case study using ORCHIDEE v1. 9.5. 2), Geoscientific Model Development, 11, 4739–4754, https://doi.org/https://gmd.copernicus.org/articles/11/4739/2018/, 2018.

Best, M., Pryor, M., Clark, D., Rooney, G., Essery, R., Menard, C., J.M., E., Hendry, M., Porson, A., Gedney, N., Mercado, L., Sitch, S., Blyth, E., Boucher, O., Cox, P., Grimmond, C., and Harding, R.: The Joint UK Land Environment Simulator (JULES), model description - Part 1: Energy and water fluxes, Geoscientific Model Development, 4, 677–699, 2011.

Beylat, S.: 4DEnVar ORCHIDEE: v1.0.0, https://doi.org/10.5281/zenodo.14609416, 2025.

Beylat, S., Raoult, N., Bacour, C., Douglas, N., Quaife, T., Bastrikov, V., Rayner, P. J., and Peylin, P.: Towards the assimilation of atmospheric CO_2 concentration data in a land surface model using adjoint-free variational methods, Geoscientific Model Development, 18, 7501–7527, https://doi.org/10.5194/gmd-18-7501-2025, 2025.

Bishop, C. H., Etherton, B. J., and Majumdar, S. J.: Adaptive Sampling with the Ensemble Transform Kalman Filter. Part I: Theoretical Aspects, Monthly Weather Review, 129, 420 – 436, https://doi.org/10.1175/1520-0493(2001)129<0420:ASWTET>2.0.CO;2, 2001.

Blyth, E., Arora, V., Clark, D., Dadson, S., De Kauwe, M., Lawrence, D., Melton, J., Pongratz, J., Turton, R., Yoshimura, K., and Yuan, H.: Advances in Land Surface Modeling, Current Climate Change Reports, 7, https://doi.org/10.1007/s40641-021-00171-5, 2021.

Bocquet, M. and Sakov, P.: Joint state and parameter estimation with an iterative ensemble Kalman smoother, Nonlinear Processes in Geophysics, 20, 803–818, https://doi.org/10.5194/npg-20-803-2013, 2013.

Bocquet, M. and Sakov, P.: An iterative ensemble Kalman smoother, Quarterly Journal of the Royal Meteorological Society, 140, 1521–1535, https://doi.org/https://doi.org/10.1002/qj.2236, 2014.

Boucher, O., Servonnat, J., Albright, A. L., Aumont, O., Balkanski, Y., Bastrikov, V., Bekki, S., Bonnet, R., Bony, S., Bopp, L., Braconnot, P., Brockmann, P., Cadule, P., Caubel, A., Cheruy, F., Codron, F., Cozic, A., Cugnet, D., D'Andrea, F., Davini, P., de Lavergne, C., Denvil, S., Deshayes, J., Devilliers, M., Ducharne, A., Dufresne, J. L., Dupont, E., Éthé, C., Fairhead, L., Falletti, L., Flavoni, S., Foujols, M. A., Gardoll, S., Gastineau, G., Ghattas, J., Grandpeix, J. Y., Guenet, B., Lionel, E. G., Guilyardi, E., Guimberteau, M., Hauglustaine, D., Hourdin, F., Idelkadi, A., Joussaume, S., Kageyama, M., Khodri, M., Krinner, G., Lebas, N., Levavasseur, G., Lévy, C., Li, L., Lott, F., Lurton, T., Luyssaert, S., Madec, G., Madeleine, J. B., Maignan, F., Marchand, M., Marti, O., Mellul, L., Meurdesoif, Y., Mignot, J., Musat, I., Ottlé, C., Peylin, P., Planton, Y., Polcher, J., Rio, C., Rochetin, N., Rousset, C., Sepulchre, P., Sima, A., Swingedouw, D., Thiéblemont, R., Traore, A. K., Vancoppenolle, M., Vial, J., Vialard, J., Viovy, N., and Vuichard, N.: Presentation and Evaluation of the IPSL-CM6A-LR Climate Model, Journal of Advances in Modeling Earth Systems, 12, https://doi.org/10.1029/2019MS002010, 2020.

Campolongo, F., Cariboni, J., and Saltelli, A.: Factorial Sampling Plans for Preliminary Computational Experiments, Environmental Modelling & Software, 22, 1509–1518, https://doi.org/10.1016/j.envsoft.2006.10.004, 2007.

https://doi.org/10.5194/egusphere-2026-132
Preprint. Discussion started: 23 March 2026

Clark, D., Mercado, L., Sitch, S., Jones, C., Gedney, N., Best, M., Pryor, M., Rooney, G., Essery, R., Blyth, E., Boucher, O., Harding, R., Huntingford, C., and Cox, P.: The Joint UK Land Environment Simulator (JULES), model description - Part 2: Carbon fluxes and vegetation dynamics, Geoscientific Model Development, 4, 701–722, 2011.

Collatz, G., Ball, T., Grivet, C., and Berry, J.: Physiological and environmental regulation of stomatal conductance, photosynthesis and transpiration: a model that includes a laminar boundary layer*., Agricultural and Forest Meteorology, 54, 107–136, 1991.

Collatz, G., Ribas-Carbo, M., and Berry, J.: Coupled Photosynthesis-Stomatal Conductance Model for Leaves of C4 Plants., Australian Journal of Plant Physiology, 19, 519–538, 1992.

Cooper, E., Blyth, E., Cooper, H., Ellis, R., Pinnington, E., and Dadson, S. J.: Using data assimilation to optimize pedotransfer functions using field-scale in situ soil moisture observations, Hydrology and Earth System Sciences, 25, 2445–2458, https://doi.org/10.5194/hess-25-2445-2021, 2021.

Courtier, P. and Talagrand, O.: Variational assimilation of meteorological observations with the direct and adjoint shallow-water equations, Tellus A: Dynamic Meteorology and Oceanography, 42, 531–549, https://doi.org/10.3402/tellusa.v42i5.11896, 1990.

Courtier, P., Thepaut, J.-N., and Hollingsworth, A.: A strategy for operational implementation of 4D-Var, using an incremental approach, Royal Meteorological Society, 120, 1367–1387, 1994.

Desroziers, G., Berre, L., Chapnik, B., and Poli, S.: Diagnosis of observation, background and analysis-error statistics in observation space, Quarterly Journal of the Royal Meteorological Society, 131, 3385–3396, https://doi.org/10.1256/qj.05.108, 2005.

Douglas, N.: NatalieDouglas/4DEnVar: Release for publication, https://doi.org/10.5281/zenodo.19001565, 2026.

Douglas, N., Quaife, T., and Bannister, R.: Exploring a hybrid ensemble–variational data assimilation technique (4DEnVar) with a simple ecosystem carbon model, Environmental Modelling & Software, 186, 106 361, https://doi.org/https://doi.org/10.1016/j.envsoft.2025.106361, 2025.

Eller, C. B., Rowland, L., Oliveira, R. S., Bittencourt, P. R. L., Barros, F. V., Silva, R. L., Christoffersen, B. O., Melgaço, A., Pinheiro, B. R., Almeida, C. T., and et al.: Modelling tropical forest drought responses using plant hydraulics, Earth System Dynamics, 11, 35–58, https://doi.org/10.5194/esd-11-35-2020, 2020.

Farquhar, G., von Caemmerer, S., and Berry, J.: A biochemical model of photosynthetic CO2 assimilation in leaves of C3 species., Planta, 149, 78–90, 1980.

Fisher, R. and Koven, C.: Perspectives on the Future of Land Surface Models and the Challenges of Representing Complex Terrestrial Systems, Journal of Advances in Modeling Earth Systems, 12, https://doi.org/10.1029/2018MS001453, 2020.

FLUXNET2015 Dataset: FLUXNET2015/US-Ha1 Eddy Covariance Site Data, https://fluxnet.org/doi/FLUXNET2015/US-Ha1, accessed: 2025-12-19, 2015.

Freitag, M. A., Nichols, N. K., and Budd, C. J.: L1-regularisation for ill-posed problems in variational data assimilation, PAMM - Proceedings in Applied Mathematics and Mechanics, 10, 665–668, https://doi.org/10.1002/pamm.201010324, shows that 4D-Var can be interpreted as Tikhonov (L2-norm) regularisation for variational data assimilation, 2010.

Golub, G. H., Heath, M., and Wahba, G.: Generalized cross-validation as a method for choosing a good ridge parameter, Technometrics, 21, 215–223, https://doi.org/10.1080/00401706.1979.10489751, 1979.

Gratton, S., Lawless, A. S., and Nichols, N. K.: A Regularization Approach for Weak-Constraint Variational Data Assimilation, Quarterly Journal of the Royal Meteorological Society, 133, 681–697, https://doi.org/10.1002/qj.56, 2007.

Hansen, P.: Analysis of discrete ill-posed problems by means of the L-curve, SIAM Review, 34, 561–580, https://doi.org/10.1137/1034115, 1992.

https://doi.org/10.5194/egusphere-2026-132
Preprint. Discussion started: 23 March 2026

Harper, A. B., Williams, K. E., McGuire, P. C., Duran Rojas, M. C., Hemming, D., Verhoef, A., Huntingford, C., Rowland, L., Marthews, T., Breder Eller, C., Mathison, C., Nobrega, R. L. B., Gedney, N., Vidale, P. L., Otu-Larbi, F., Pandey, D., Garrigues, S., Wright, A., Slevin, D., De Kauwe, M. G., Blyth, E., Ardö, J., Black, A., Bonal, D., Buchmann, N., Burban, B., Fuchs, K., de Grandcourt, A., Mammarella, I., Merbold, L., Montagnani, L., Nouvellon, Y., Restrepo-Coupe, N., and Wohlfahrt, G.: Improvement of modeling plant responses to low soil moisture in JULESvn4.9 and evaluation against flux tower measurements, Geoscientific Model Development, 14, 3269–3294, https://doi.org/10.5194/gmd-14-3269-2021, 2021.

Harris, I., Osborn, T. J., Jones, P., and Lister, D.: Version 4 of the CRU TS monthly high-resolution gridded multivariate climate dataset, Scientific Data, 7, https://doi.org/10.1038/s41597-020-0453-3, 2020.

Jacobs, C. M. J.: Direct impact of atmospheric CO_2 enrichment on regional transpiration, PhD Thesis, Wageningen Agricultural University, 1994.

Kaminski, T., Knorr, W., Rayner, P. J., and Heimann, M.: Assimilating atmospheric data into a terrestrial biosphere model: A case study of the seasonal cycle, Global Biogeochemical Cycles, 16, https://doi.org/10.1029/2001gb001463, 2002.

Kattge, J. and Knorr, W.: Temperature acclimation in a biochemical model of photosynthesis: a reanalysis of data from 36 species, Plant, Cell & Environment, 30, 1176–1190, https://doi.org/https://doi.org/10.1111/j.1365-3040.2007.01690.x, 2007.

Kobayashi, S., Ota, Y., Harada, Y., Ebita, A., Moriya, M., Onoda, H., Onogi, K., Kamahori, H., Kobayashi, C., Endo, H., Miyaoka, K., and Kiyotoshi, T.: The JRA-55 reanalysis: General specifications and basic characteristics, Journal of the Meteorological Society of Japan, 93, https://doi.org/10.2151/jmsj.2015-001, 2015.

Krinner, G., Viovy, N., de Noblet-Ducoudre, N., Ogee, J., Polcher, J., Friedlingstein, P., Ciais, P., Sitch, S., and Prentice, C.: A dynamic global vegetation model for studies of the coupled atmosphere-biosphere system, Global Biogeochemical Cycles, 19, https://doi.org/10.1029/2003GB002 199, 2005.

Kuppel, S., Peylin, P., Chevallier, F., Bacour, C., Maignan, F., and Richardson, A. D.: Constraining a global ecosystem model with multi-site eddy-covariance data, Biogeoscience, 9, 3757–3776, https://doi.org/10.5194/bg-9-3757-2012, 2012.

Liu, C. and Xiao, Q.: An Ensemble-Based Four-Dimensional Variational Data Assimilation Scheme. Part III: Antarctic Applications with Advanced Research WRF Using Real Data, Monthly Weather Review, 141, 2721 – 2739, https://doi.org/10.1175/MWR-D-12-00130.1, 2013.

Liu, C., Xiao, Q., and Wang, B.: An ensemble-based four-dimensional variational data assimilation scheme. Part I: Technical formation and preliminary test., Monthly Weather Review, 136, 3363–3373, 2008.

Lorenc, A. C.: Modelling of error covariances by 4D-Var data assimilation, Quarterly Journal of the Royal Meteorological Society, 129, 3167–3182, 2003.

Medlyn, B. E., Duursma, R. A., Eamus, D., Ellsworth, D. S., Prentice, I. C., Barton, C. V., Crous, K. Y., De angelis, P., Freeman, M., and Wingate, L.: Reconciling the optimal and empirical approaches to modelling stomatal conductance., Global Change Biology, 17, 2134–2144, https://doi.org/https://doi.org/10.1111/j.1365-2486.2012.02790.x, 2011.

Medlyn, B. E., Duursma, R. A., Eamus, D., Ellsworth, D. S., Prentice, I. C., Barton, C. V., Crous, K. Y., De angelis, P., Freeman, M., and Wingate, L.: Reconciling the optimal and empirical approaches to modelling stomatal conductance., Global Change Biology, 18, 3476–3476, https://doi.org/https://doi.org/10.1111/j.1600-0889.2007.00256.x, 2012.

Morozov, V. A.: Methods for Solving Incorrectly Posed Problems, Springer, New York, https://doi.org/10.1007/978-1-4612-5280-1, translated from Russian by A. B. Aries, 1984.

https://doi.org/10.5194/egusphere-2026-132
Preprint. Discussion started: 23 March 2026

Morris, M.: An effective screening design for sensitivity analysis of large models, Technometrics, 33, 161–174, https://doi.org/10.2307/1269043, 1991.

ORCHIDEE: ORCHIDEE V22 r7878 gmd 2025 4DEnVar, https://doi.org/10.14768/c68bc728-da71-4383-84df-dcde31d9c006, 2025.

Pastorello, G., Trotta, C., Canfora, E., Chu, H., Christianson, D., Cheah, Y.-W., Poindexter, C., Chen, J., Elbashandy, A., Humphrey, M., Isaac, P., Polidori, D., Reichstein, M., Ribeca, A., van Ingen, C., Vuichard, N., Zhang, L., Amiro, B., Ammann, C., Arain, M. A., Ardö, J., Arkebauer, T., Arndt, S. K., Arriga, N., Aubinet, M., Aurela, M., Baldocchi, D., Barr, A., Beamesderfer, E., Marchesini, L. B., Bergeron, O., Beringer, J., Bernhofer, C., Berveiller, D., Billesbach, D., Black, T. A., Blanken, P. D., Bohrer, G., Boike, J., Bolstad, P. V., Bonal, D., Bonnefond, J.-M., Bowling, D. R., Bracho, R., Brodeur, J., Brümmer, C., Buchmann, N., Burban, B., Burns, S. P., Buysse, P., Cale, P., Cavagna, M., Cellier, P., Chen, S., Chini, I., Christensen, T. R., Cleverly, J., Collalti, A., Consalvo, C., Cook, B. D., Cook, D., Coursolle, C., Cremonese, E., Curtis, P. S., D'Andrea, E., da Rocha, H., Dai, X., Davis, K. J., Cinti, B. D., Grandcourt, A. d., Ligne, A. D., De Oliveira, R. C., Delpierre, N., Desai, A. R., Di Bella, C. M., Tommasi, P. d., Dolman, H., Domingo, F., Dong, G., Dore, S., Duce, P., Dufrêne, E., Dunn, A., Dušek, J., Eamus, D., Eichelmann, U., ElKhidir, H. A. M., Eugster, W., Ewenz, C. M., Ewers, B., Famulari, D., Fares, S., Feigenwinter, I., Feitz, A., Fensholt, R., Filippa, G., Fischer, M., Frank, J., Galvagno, M., Gharun, M., Gianelle, D., Gielen, B., Gioli, B., Gitelson, A., Goded, I., Goeckede, M., Goldstein, A. H., Gough, C. M., Goulden, M. L., Graf, A., Griebel, A., Gruening, C., Grünwald, T., Hammerle, A., Han, S., Han, X., Hansen, B. U., Hanson, C., Hatakka, J., He, Y., Hehn, M., Heinesch, B., Hinko-Najera, N., Hörtnagl, L., Hutley, L., Ibrom, A., Ikawa, H., Jackowicz-Korczynski, M., Janouš, D., Jans, W., Jassal, R., Jiang, S., Kato, T., Khomik, M., Klatt, J., Knohl, A., Knox, S., Kobayashi, H., Koerber, G., Kolle, O., Kosugi, Y., Kotani, A., Kowalski, A., Kruijt, B., Kurbatova, J., Kutsch, W. L., Kwon, H., Launiainen, S., Laurila, T., Law, B., Leuning, R., Li, Y., Liddell, M., Limousin, J.-M., Lion, M., Liska, A. J., Lohila, A., López-Ballesteros, A., López-Blanco, E., Loubet, B., Loustau, D., Lucas-Moffat, A., Lüers, J., Ma, S., Macfarlane, C., Magliulo, V., Maier, R., Mammarella, I., Manca, G., Marcolla, B., Margolis, H. A., Marras, S., Massman, W., Mastepanov, M., Matamala, R., Matthes, J. H., Mazzenga, F., McCaughey, H., McHugh, I., McMillan, A. M. S., Merbold, L., Meyer, W., Meyers, T., Miller, S. D., Minerbi, S., Moderow, U., Monson, R. K., Montagnani, L., Moore, C. E., Moors, E., Moreaux, V., Moureaux, C., Munger, J. W., Nakai, T., Neirynck, J., Nesic, Z., Nicolini, G., Noormets, A., Northwood, M., Nosetto, M., Nouvellon, Y., Novick, K., Oechel, W., Olesen, J. E., Ourcival, J.-M., Papuga, S. A., Parmentier, F.-J., Paul-Limoges, E., Pavelka, M., Peichl, M., Pendall, E., Phillips, R. P., Pilegaard, K., Pirk, N., Posse, G., Powell, T., Prasse, H., Prober, S. M., Rambal, S., Rannik, Ü., Raz-Yaseef, N., Rebmann, C., Reed, D., Dios, V. R. d., Restrepo-Coupe, N., Reverter, B. R., Roland, M., Sabbatini, S., Sachs, T., Saleska, S. R., Sánchez-Cañete, E. P., Sanchez-Mejia, Z. M., Schmid, H. P., Schmidt, M., Schneider, K., Schrader, F., Schroder, I., Scott, R. L., Sedlák, P., Serrano-Ortíz, P., Shao, C., Shi, P., Shironya, I., Siebicke, L., Šigut, L., Silberstein, R., Sirca, C., Spano, D., Steinbrecher, R., Stevens, R. M., Sturtevant, C., Suyker, A., Tagesson, T., Takanashi, S., Tang, Y., Tapper, N., Thom, J., Tomassucci, M., Tuovinen, J.-P., Urbanski, S., Valentini, R., van der Molen, M., van Gorsel, E., van Huissteden, K., Varlagin, A., Verfaillie, J., Vesala, T., Vincke, C., Vitale, D., Vygodskaya, N., Walker, J. P., Walter-Shea, E., Wang, H., Weber, R., Westermann, S., Wille, C., Wofsy, S., Wohlfahrt, G., Wolf, S., Woodgate, W., Li, Y., Zampedri, R., Zhang, J., Zhou, G., Zona, D., Agarwal, D., Biraud, S., Torn, M., and Papale, D.: The FLUXNET2015 dataset and the ONEFlux processing pipeline for eddy covariance data, Scientific Data, 7, 225, https://doi.org/10.1038/s41597-020-0534-3, 2020.

Peters, W., Miller, J. B., Whitaker, J., Denning, A. S., Hirsch, A., Krol, M. C., Zupanski, D., Bruhwiler, L., and Tans, P. P.: An ensemble data assimilation system to estimate CO2 surface fluxes from atmospheric trace gas observations, Journal of Geophysical Research: Atmospheres, 110, https://doi.org/https://doi.org/10.1029/2005JD006157, 2005.

https://doi.org/10.5194/egusphere-2026-132
Preprint. Discussion started: 23 March 2026

Peylin, P., Bacour, C., MacBean, N., Leonard, S., Rayner, P., Kuppel, S., Koffi, E., Kane, A., Maignan, F., Chevallier, F., Ciais, P., and Prunet, P.: A new stepwise carbon cycle data assimilation system using multiple data streams to constrain the simulated land surface carbon cycle, Geoscientific Model Development, 9, 3321–3346, https://doi.org/10.5194/gmd-9-3321-2016, 2016.

Pinnington, E., Quaife, T., Lawless, A., Williams, K., Arkebauer, T., and Scoby, D.: The Land Variational Ensemble Data Assimilation Framework: LAVENDAR v1.0.0, Geoscientific Model Development, 9, 55–69, 2020.

Pinnington, E., Amezcua, J., Cooper, E., Dadson, S., Ellis, R., Peng, J., Robinson, E., Morrison, R., Osborne, S., and Quaife, T.: Improving soil moisture prediction of a high-resolution land surface model by parameterising pedotransfer functions through assimilation of SMAP satellite data, Hydrology and Earth System Sciences, 25, 1617–1641, https://doi.org/10.5194/hess-25-1617-2021, 2021.

Posselt, D. J. and Bishop, C. H.: Nonlinear Parameter Estimation: Comparison of an Ensemble Kalman Smoother with a Markov Chain Monte Carlo Algorithm, Monthly Weather Review, 140, 1957 – 1974, https://doi.org/10.1175/MWR-D-11-00242.1, 2012.

Raoult, N., Douglas, N., MacBean, N., Kolassa, J., Quaife, T., Roberts, A. G., Fisher, R., Fer, I., Bacour, C., Dagon, K., Hawkins, L., Carvalhais, N., Cooper, E., Dietze, M. C., Gentine, P., Kaminski, T., Kennedy, D., Liddy, H. M., Moore, D. J. P., Peylin, P., Pinnington, E., Sanderson, B., Scholze, M., Seiler, C., Smallman, T. L., Vergopolan, N., Viskari, T., Williams, M., and Zobitz, J.: Parameter Estimation in Land Surface Models: Challenges and Opportunities With Data Assimilation and Machine Learning, Journal of Advances in Modeling Earth Systems, 17, e2024MS004 733, https://doi.org/https://doi.org/10.1029/2024MS004733, e2024MS004733 2024MS004733, 2025.

Raoult, N. M., Jupp, T. E., Cox, P. M., and Luke, C. M.: Land-surface parameter optimisation using data assimilation techniques: The adJULES system V1.0, Geoscientific Model Development, 9, https://doi.org/10.5194/gmd-9-2833-2016, 2016.

Rawlins, F., Ballard, S., Bovis, K. J., Clayton, A. M., Li, D., Inverarity, G. W., Lorenc, A. C., and Payne, T. J.: The Met Office global four-dimensional variational data assimilation scheme, Royal Meteorological Society, 133, 347–362, 2007.

Rayner, P. J., Scholze, M., Knorr, W., Kaminski, T., Giering, R., and Widmann, H.: Two decades of terrestrial carbon fluxes from a carbon cycle data assimilation system (CCDAS), Global Biogeochemical Cycles, 19, https://doi.org/10.1029/2004GB002254, 2005.

Reynolds, C. A., Jackson, T. J., and Rawls, W. J.: Estimating soil water-holding capacities by linking the Food and Agriculture Organization soil map of the world with global pedon databases and continuous pedotransfer functions, Water Resources Research, 36, https://doi.org/10.1029/2000WR900130, 2000.

Santaren, D., Peylin, P., Viovy, N., and Ciais, P.: Optimizing a process-based ecosystem model with eddy-covariance flux measurements: A pine forest in southern France, Global Biogeochemical Cycles, 21, https://doi.org/10.1029/2006GB002834, 2007.

Sitch, S., O'Sullivan, M., Robertson, E., Friedlingstein, P., Albergel, C., Anthoni, P., Arneth, A., Arora, V. K., Bastos, A., Bastrikov, V., Bellouin, N., Canadell, J. G., Chini, L., Ciais, P., Falk, S., Harris, I., Hurtt, G., Ito, A., Jain, A. K., Jones, M. W., Joos, F., Kato, E., Kennedy, D., Klein Goldewijk, K., Kluzek, E., Knauer, J., Lawrence, P. J., Lombardozzi, D., Melton, J. R., Nabel, J. E. M. S., Pan, N., Peylin, P., Pongratz, J., Poulter, B., Rosan, T. M., Sun, Q., Tian, H., Walker, A. P., Weber, U., Yuan, W., Yue, X., and Zaehle, S.: Trends and Drivers of Terrestrial Sources and Sinks of Carbon Dioxide: An Overview of the TRENDY Project, Global Biogeochemical Cycles, 38, e2024GB008 102, https://doi.org/https://doi.org/10.1029/2024GB008102, e2024GB008102 2024GB008102, 2024.

Visweshwaran, R., Cooper, E., and Dance, S.: Improving JULES Soil Moisture Estimates through 4D-En-Var Hybrid Assimilation of COSMOS-UK Soil Moisture Observations., EGUsphere [preprint], https://doi.org/https://doi.org/10.5194/egusphere-2024-3980, 2025.

Wang, Y. P., Leuning, R., Cleugh, H. A., and Coppin, P. A.: Parameter estimation in surface exchange models using nonlinear inversion: How many parameters can we estimate and whichmeasurements are most useful?, Global Change Biology, 7, https://doi.org/10.1046/j.1365-2486.2001.00434.x, 2001.

https://doi.org/10.5194/egusphere-2026-132
Preprint. Discussion started: 23 March 2026

Williams, K. D., Copsey, D., Blockley, E. W., Bodas-Salcedo, A., Calvert, D., Comer, R., Davis, P., Graham, T., Hewitt, H. T., Hill, R., Hyder, P., Ineson, S., Johns, T. C., Keen, A. B., Lee, R. W., Megann, A., Milton, S. F., Rae, J. G., Roberts, M. J., Scaife, A. A., Schiemann, R., Storkey, D., Thorpe, L., Watterson, I. G., Walters, D. N., West, A., Wood, R. A., Woollings, T., and Xavier, P. K.: The Met Office Global Coupled Model 3.0 and 3.1 (GC3.0 and GC3.1) Configurations, Journal of Advances in Modeling Earth Systems, 10, https://doi.org/10.1002/2017MS001115, 2018.

Xu, Q., Wei, L., and Gu, C.: Optimal Estimation of Background-Error Covariance Parameters for Doppler Radar Wind Analysis Using the L-Curve Method, Journal of Atmospheric and Oceanic Technology, 23, 1108–1122, https://doi.org/10.1175/JTECH1902.1, 2006.

Yin, X. and Struik, P. C.: C3 and C4 photosynthesis models: An overview from the perspective of crop modelling, NJAS: Wageningen Journal of Life Sciences, 57, 27–38, https://doi.org/10.1016/j.njas.2009.07.001, 2009.